

# Applications of Adaptive Time - Frequency Representations to Underwater Acoustic Signal Processing

Richard Baraniuk and Doug Jones  
 Dept. of Electrical and Computer Engineering  
 University of Illinois  
 Urbana, IL 61801

Tom Brotherton and Larry Marple  
 The ORINCON Corp.  
 9363 Towne Centre Drive  
 San Diego, CA 92121

## Abstract

*There is currently an interest in underwater signal processing to perform detection and classification of transient acoustic events. Traditional FFT based sonar signal processing techniques are not well suited for processing many transient signals of concern, particularly those of short duration and nonstationary nature. Described here is the application of an Adaptive-Optimal-Kernel (AOK) Time-Frequency Representation to the problem. The AOK technique employs a radially-Gaussian signal-dependent smoothing kernel obtained by solving an optimization problem and is ideal for characterizing many acoustic signals of interest. Examples are given which demonstrate the effectiveness of the approach for simulated and real sonar data.*

## 1 Introduction

There is currently an interest in underwater signal processing to perform detection and classification of unknown, transient acoustic events. Traditional sonar signal processing techniques (i.e., FFT based algorithms) are not well suited for processing many transient signals of concern, particularly those of short duration and nonstationary nature [1]. Impulsive events and chirp type signals such as biologic clicks and squeals, underwater explosions, and the operation of mechanical devices, in particular, are not well modeled by standard FFT processing techniques.

Described here is the application of an Adaptive-Optimal-Kernel (AOK) Time-Frequency Representation (TFR), developed by Baraniuk and Jones [2], to the processing of short duration, nonstationary underwater acoustic events. Current bilinear time-frequency representations such as the Wigner [3], Choi-Williams [4], and ZAM-kernel [5] distributions apply a fixed kernel to smooth the cross-components which can obscure the true signal features and complicate interpretation of the representation. Unfortunately, selection of a fixed kernel limits the class of signals that can be analyzed effectively.

To overcome this limitation, the AOK uses a radially-Gaussian *signal-dependent* kernel that changes shape to optimally smooth the distribution [2].

The optimal kernel,  $\Phi$ , for a signal is defined as the solution to the following optimization problem:

$$\max_{\Phi} \int_0^{2\pi} \int_0^{\infty} |A(r, \psi) \Phi(r, \psi)|^2 r dr d\psi \quad (1)$$

subject to

$$\Phi(r, \psi) = e^{-\frac{r^2}{2\sigma^2(\psi)}} \quad (2)$$

$$\frac{1}{2\pi} \int_0^{2\pi} \int_0^{\infty} |\Phi(r, \psi)|^2 r dr d\psi \leq \alpha, \quad \alpha \geq 0 \quad (3)$$

$A$  is the ambiguity function (AF) of the signal in polar coordinates. Once the optimal kernel is computed, the AOK Time / Frequency Representation is given by

$$P(t, \omega) = \frac{1}{2\pi} \int_{-\infty}^{\infty} \int_{-\infty}^{\infty} A(\theta, \tau) \Phi(\theta, \tau) e^{-j\theta t - j\tau \omega} d\theta d\tau \quad (4)$$

The AOK is ideal for characterizing many acoustic transient signals of interest. Details of the AOK technique are presented in section 2. Application of the AOK technique to both real and simulated data is presented in section 3. The examples demonstrate the effectiveness of the signal-dependent approach and allow for comparison against other fixed-kernel techniques. Section 4 contains conclusions and a summary of results.

## 2 The Radially-Gaussian Signal-Dependent Representation

The signal-dependent kernel design procedure is formulated as an optimization problem. In general, the problem formulation involves the signal, and includes a set of constraints that define a class of kernels from which the optimal kernel is chosen, and a performance index

that measures the quality of the time-frequency representation for each kernel. The kernel that maximizes the value of the performance measure is selected as the optimal kernel for the signal. Possible constraints could include, for example, constraints that force the kernel to suppress cross-components, and to satisfy the marginal distributions [4]. Clearly, the choice of constraints and performance measure is crucial to the success of the method. However, once a satisfactory set of constraints and measure are found, kernel design for a wide range of signals reduces to solving an optimization problem.

A method for optimal, signal-dependent kernel design is discussed in [6]. In that paper, the constraints force the kernel to be bounded, radially nonincreasing and of finite volume, that is, to be a two-dimensional lowpass filter, while the performance index measures the energy passed from the AF into the TFR. The optimal kernel was shown to yield excellent results for a variety of signals. A fundamental property of this technique is that the optimal kernel is a 1/0 mask, and, hence, can introduce ringing into the TFR. To overcome this problem, a new kernel design procedure using radially-Gaussian functions was introduced in [2]. This class of kernels is inherently tapered, and may potentially yield more desirable results for many signals.

The signal-dependent radially-Gaussian kernel in the  $(\theta, \tau)$ -plane is defined as :

$$\Phi(\theta, \tau) = e^{-\frac{\theta^2 + \tau^2}{2\sigma^2(\psi)}} \quad (5)$$

where  $\sigma$  is a parameter which measures spread and varies with radial angle  $\psi$ .

The shape of the kernel is completely parameterized by the positive, one-dimensional function  $\sigma$ , so finding the optimal, radially-Gaussian kernel for a signal is equivalent to finding the optimal function,  $\sigma(\psi)$ , for the signal. Since  $\sigma(\psi)$  controls the spread along a radial slice of the kernel at angle  $\psi$ , we call it the *spread function*. Clearly, if  $\sigma$  is smooth, then  $\Phi$ , is also smooth. The kernel is easily expressed in polar coordinates by using  $r = (\theta^2 + \tau^2)^{1/2}$  as the radius variable:

$$\Phi(r, \psi) = e^{-\frac{r^2}{2\sigma^2(\psi)}} \quad (6)$$

In practice, TFR's are computed at discrete time and frequency locations. The polar-sampled, radially-Gaussian kernel is given by

$$\Phi_p(p, q) = e^{-\frac{(p\Delta_r)^2}{2\sigma^2(q\Delta_\psi)}} \quad (7)$$

$p=0, \dots, P-1, \text{ and } q=0, \dots, Q-1$

where  $p$  and  $q$  are the radius and angle indices, and  $\Delta_r$  and  $\Delta_\psi$  are the radius and angle step sizes. The discrete kernel

is parameterized by a positive spread vector,  $\underline{\sigma}$ , whose elements correspond to samples of the spread function

$$\sigma_q = \sigma(q\Delta_\psi). \quad (8)$$

We define the optimal discrete kernel as the radially-Gaussian function whose spread vector solves the following optimization problem:

$$\max_{\Phi, \underline{\sigma}} \Delta_r^2 \Delta_\psi \sum_{q=0}^{Q-1} \sum_{p=1}^{P-1} p |A_p(p, q) \Phi_p(p, q)|^2 \quad (9)$$

subject to

$$\Phi_p(p, q) = e^{-\frac{(p\Delta_r)^2}{2\sigma_q^2}} \quad (10)$$

$$\frac{\Delta_\psi}{2\pi} \sum_{q=0}^{Q-1} \sigma_q^2 \leq \alpha, \quad \alpha \geq 0 \quad (11)$$

The constraints and performance index are motivated by a desire to suppress cross-components, and pass auto-components with as little distortion as possible. The first constraint (10) limits the signal-dependent kernel to the class of radially-Gaussian kernels. Thus, the kernel is constrained to be a lowpass filter. Since the AF auto-components are centered at the origin, this encourages the kernel to preferentially pass auto-components. The second constraint (11) limits the volume of the kernel to  $\alpha$ , so that cross-components are suppressed. The performance measure (9) expresses a desire to minimize auto-component distortion by passing as much auto-component energy as possible into the TFR for a kernel of fixed volume. An advantage of this formulation is that the constraints are insensitive to both the time-scale and orientation of the signal in time-frequency.

The computation of the discrete, optimal-kernel TFR requires samples of the AF on a polar grid,  $A_p(p, q)$ . These are computed either directly, or via interpolation from a rectangularly-sampled AF. Solving the optimization problem (9)-(11) for the optimal spread vector,  $\underline{\sigma}^*$ , determines polar samples of a radially-Gaussian kernel,  $\Phi_p$ . Interpolation of the kernel to a rectangular grid and multiplication by the rectangularly-sampled AF yields the characteristic function, whose two-dimensional discrete Fourier transform is the optimal-kernel TFR.

The constrained optimization problem (9)-(11) that defines the optimal kernel is nonlinear in the variables  $\sigma_q$ . The solution is computed using a simple iterative solution algorithm that is based on the principle of gradient ascent, with an additional projection step that ensures that the volume constraint (11) remains satisfied.

### 3 Application to Underwater Acoustic Data

To demonstrate and compare the AOK time / frequency representation with other representations, a simulation was performed. A test data set was generated that was made up of a sequence of signals each of which contains chirps. There are three signals in the data. Each of the simulated signal lasts for 256 samples and is separated from adjacent signals by 256 samples of zeroes. The first signal contains a single chirp. The second signal contains two chirps that have the same chirp rate but are separated in frequency. The third signal contains crossing chirps. Figure 1(e) shows the signal structure in time and frequency.

Simulated white Gaussian noise of varying amplitude levels was then added to the data to generate a received signal at various signal to noise ratios (SNRs). The simulated data was then processed to produce the AOK TFR as well as the STFT spectrum, the Wigner distribution and the ZAM distribution. Figures 1 and 2 shows input signal as well as contour plots for each of the time frequency representations for the same set of signals at two different SNRs. The levels of the contour plots were selected by hand. Parameter settings for each of the techniques were chosen so as to give good results.

Figure 1, the high SNR case, highlights the properties of each of the techniques. The STFT (figure 1(b)) picks up the gross features of the signal, but at a low frequency resolution which is required to track the chirps with the STFT. The STFT does not resolve the two chirps in the second signal. The Wigner distribution (figure 1(c)) has better performance in that frequency estimates are of relatively high resolution. However, the plot contains many artifacts. The ZAM TFR (figure 1(d)) does a good job of tracking the signals and gives relatively high resolution estimates. However the two chirps in the second signal are not resolved. It is clear, however, that the second signal is more complicated than a single chirp. The AOK TFR (figure 1(e)) reproduces the simulated data time / frequency structure exactly.

Figure 2 shows the same set of plots, but now for the low SNR case. The results are dramatic. The signals can still be seen in the STFT and ZAM TFR with some noise coming through. The signals are completely lost in the Wigner TFR. The AOK TFR still gives an almost perfect representation of the signals.

The method was then applied to actual at-sea recorded sonar data shown in figures 3 and 4. The events here are due to man-made operations that result in an impulsive signals shown in figures 3(a) and 4(a). As seen in figure 3, there are no significant differences that can be seen between the STFT, ZAM, and AOK TFRs. The most dramatic results correspond to figure 4. As seen, the AOK TFR (figure 4(e)) indicates that the impulsive signal is made up of three different chirped signal. This signal structure can not be seen in the other TFRs.

For classification of the signal shown in figure 4(a), the AOK TFR gives a unique, unambiguous representation of the signal when compared with the other TFRs. This particularly true if the problem at hand is to use the TFRs as features for classification. It may also offer insight into determining the mechanisms that give rise to signals as shown in figure 4(a).

### 4 Conclusions

In this paper we have described the application an Adaptive Optimal Kernel Time /Frequency Representation to the processing of underwater acoustic data. The optimal kernel is a signal-dependent radially-Gaussian function. The simulations presented indicate that the technique should work well for a larger set of signal classes than any current fixed-kernel representation. The technique has excellent performance even in the presence of substantial additive noise. This property may be exploited for signal detection. The AOK technique appears to offer unique features that can be used to characterize and automatically classify signals of interest, particularly true when compared to other processing techniques.

### References

- [1] S.L.Marple and T.W.Brotherton, Detection and Classification of Short Duration Underwater Acoustic Signals by Prony's Method, *IEEE ICASSP '91*, May 1991.
- [2] R.G.Baraniuk and D.L.Jones, A Radially Gaussian, Signal-Dependent Time-Frequency Representation, *IEEE ICASSP '91*, May 1991.
- [3] P.Flandrin, Some Features of Time-Frequency Representations of Multicomponent Signals, *IEEE ICASSP-1984*, pp. 41. B. 4. 1--41. B. 4. 4, 1984.
- [4] H.-I.Choi and W.J.Williams, Improved Time-Frequency Representation of Multicomponent Signals Using Exponential Kernels, *IEEE Transactions on Acoustics, Speech, and Signal Processing ASSP-37* (6), pp. 862--871, June 1989.
- [5] Y.Zhao, L.E.Atlas, and R.J.Marks, The Use of Cone-Shaped Kernels for Generalized Time-Frequency Representations of Nonstationary Signal, *IEEE Transactions on Acoustics, Speech, and Signal Processing ASSP-38* (7), pp. 1084--1091, July 1990.
- [6] R.G.Baraniuk and D.L.Jones. Optimal Kernels for Time-Frequency Analysis, *SPIE 1990 Symposium on Optical and Optoelectronic Applied Science and Engineering*, San Diego,California, July 8--13, 1990.

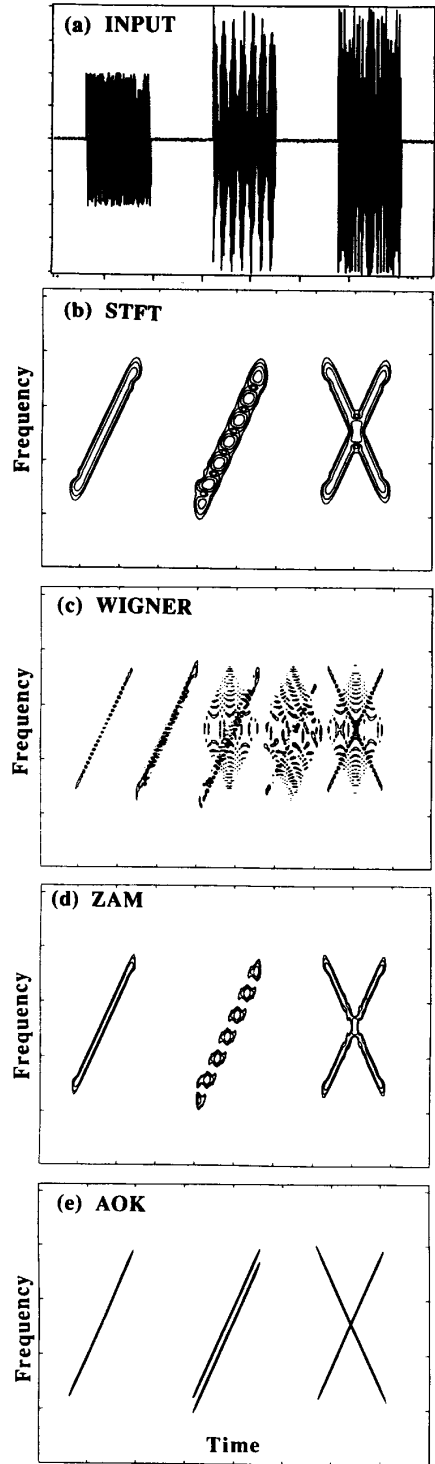


Figure 1 - High SNR Simulation

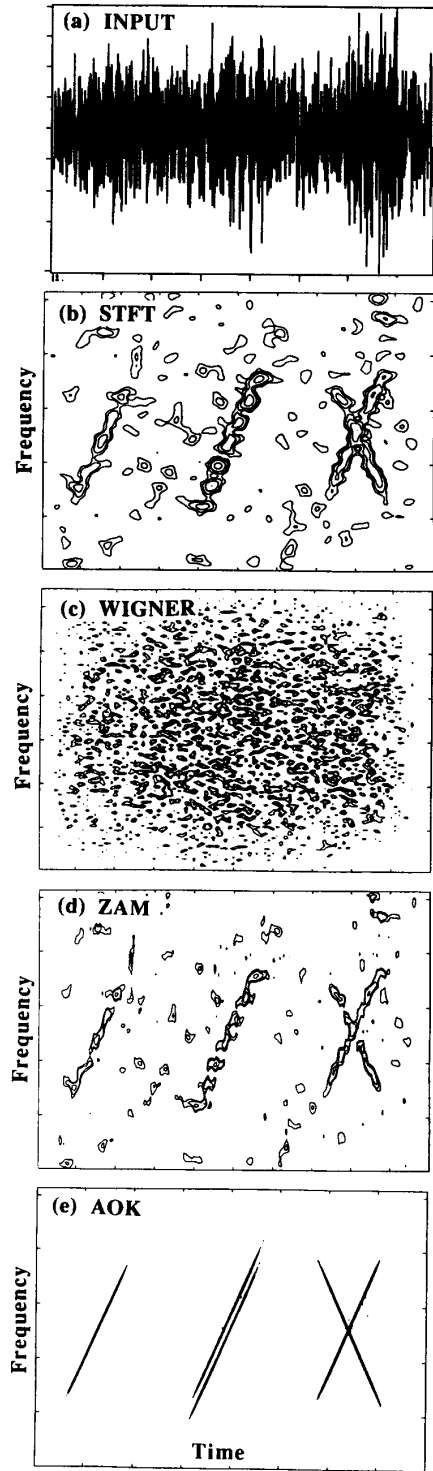


Figure 2 - Low SNR Simulation

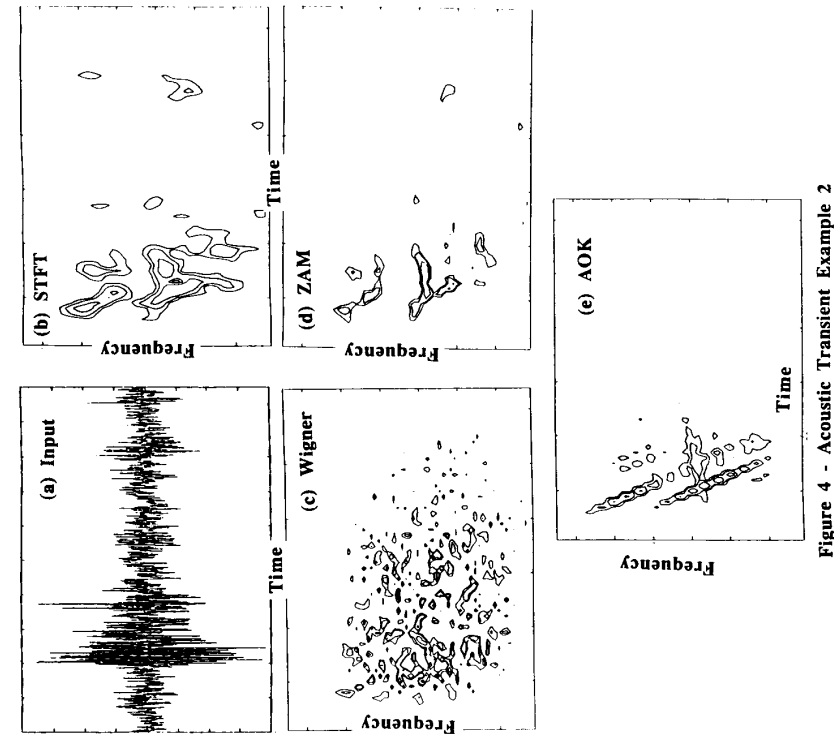


Figure 3 - Acoustic Transient Example 1

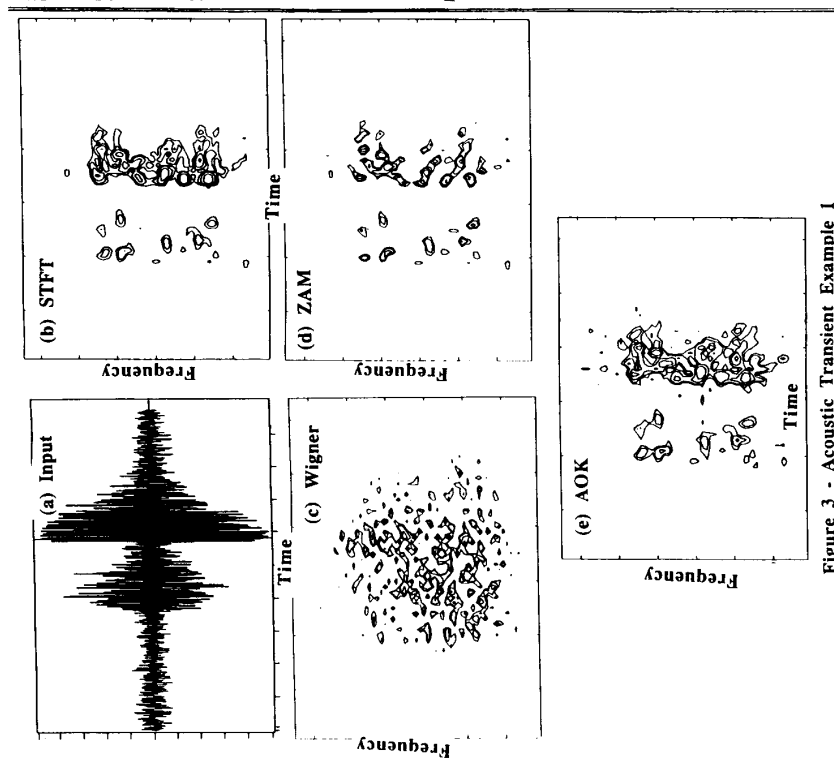


Figure 4 - Acoustic Transient Example 2